Journal of Materials Science: Materials in Electronics (2019) 30:19618–19624
https://doi.org/10.1007/s10854-019-02335-4

Effect of Zn substitution on the structure and magnetic properties of $Sr_{0.1}La_{0.45}Ca_{0.45}Fe_{11.7-x}Zn_xCo_{0.3}O_{19}$ hexagonal ferrites

Jiao Du[1] · Lixian Lian[1] · Ying Liu[1] · Yibo Du[1]

Received: 21 April 2019 / Accepted: 3 October 2019 / Published online: 18 October 2019

Abstract
M-type strontium ferrites $Sr_{0.1}La_{0.45}Ca_{0.45}Fe_{11.7-x}Zn_xCo_{0.3}O_{19}$ ($x=0$, 0.05, 0.1, 0.15 and 0.2) were synthesized by ceramic process. The effects of Zn substitution on phase composition, microstructure, sublattice occupation and magnetic properties of the ferrites were systematically investigated using X-ray diffraction, field emission scanning electron microscopy, ^{57}Fe Mössbauer spectroscopy and magnetic properties test instrument, respectively. The results showed that all the samples were single hexagonal ferrite phase with no observation of other phases, while the lattice constant a did not vary basically and the lattice constant c increased continuously with increase of the Zn substitution amount. Simultaneously, the FESEM micrographs showed that more platelet shaped grains were observed. Mössbauer spectra have revealed that Zn^{2+} ions occupied both $4f_1$ and $4f_2$ sites, but Zn^{2+} ions would prefer to occupying $4f_2$ site with increasing Zn substitution. In addition, the remanence (B_r) of the sintered ferrites increased firstly and then decreased, while the intrinsic coercivity (H_{cj}) decreased continuously. The sintered ferrites with the optimal Zn doping level of $x=0.05$ exhibited high magnetic properties, including $B_r=439.7$ mT, $H_{cj}=371.8$ kA/m and $(BH)_{max}=36.88$ kJ/m^3.

1 Introduction

M-type hexagonal ferrites have been widely used in household appliances, cars, communication equipment, medical facility, military industry, and aviation owing to the abundance of raw materials, low cost, excellent chemical stability, relatively high remanence, and large coercivity [1–3]. Much research in recent years has been made to meet the increasing demand of market and the improvement of magnetic property requirements by adding or replacing some elements. For example, interests have been focused on the substitution of Sr^{2+} by La^{3+}, Nd^{3+}, Sm^{3+}, Ca^{2+} etc, Fe^{3+} by Co^{2+}, Cr^{3+}, Al^{3+}, Bi^{3+}, Zn^{2+} [4–11], etc., and various cation combinations such as La–Co, La–Zn, La–Cu, Mn–Zn, Nd–Co [12–20], as reported. The change of the intrinsic magnetic properties of the substituted ferrites is related with the variation of the atomic magnetic moments and especially the magneto-crystalline anisotropy field [21–24].

It is reported that appropriate La–Co–Ca co-substitution can dramatically improve the magnetic properties in the $Sr_{1-x-y}La_xCa_yFe_{11.7-z}Co_zO_{19}$ ($0.39\le x\le 0.45$, $0.2\le y\le 0.25$, $0.3\le z\le 0.35$) ferrites [25–28]. La–Co substituted strontium ferrites with La/Co ratio ranging from 1.2 to 1.67 attract interests due to the fact that the powders are of single M-type phase and could improve magnetic properties [13, 24]. At present, most of commercial hexagonal ferrites with excellent magnetic properties are the La–Co–Ca substituted strontium ferrites. Calcium and strontium have the similar electronic configuration due to belonging to the same principal family in periodic table. Moreover, $CaCO_3$ has lower costs and richer reserves, compared with $SrCO_3$. It has been reported that the substitution of non-magnetic Zn^{2+} ions for partial Fe^{3+} ions at the down spin sites can enhance the saturation magnetization of the ferrites [11, 14, 30]. Therefore, in this work, an approach of Zn^{2+} substitution on the basis of La–Co–Ca co-substituted strontium ferrites was employed to further improve the magnetization, which so far has been rarely reported. Thus, we have prepared $Sr_{0.1}La_{0.45}Ca_{0.45}Fe_{11.7-x}Zn_xCo_{0.3}O_{19}$ ferrites through ceramic process. The effect of Zn^{2+} substitution on the structure and magnetic properties of $Sr_{0.1}La_{0.45}Ca_{0.45}Fe_{11.7-x}Zn_xCo_{0.3}O_{19}$ hexagonal ferrites has been investigated systematically.

✉ Ying Liu
liuying5536@163.com

[1] College of Materials Science and Engineering, Sichuan University, Chengdu 610065, China

2 Experimental

M-type hexagonal ferrite $Sr_{0.1}La_{0.45}Ca_{0.45}Fe_{11.7-x}Zn_xCo_{0.3}O_{19}$ ($x=0$, 0.05, 0.1, 0.15, 0.2) were prepared via a solid-state reaction method. In this study, the raw materials, $SrCO_3$ (97%, purity), Fe_2O_3 (98.4%, purity), La_2O_3 (99%, purity), Co_2O_3 (99%, purity), $CaCO_3$ (99%, purity), and ZnO (99%, purity) were accurately weighed according to the chemical composition of $Sr_{0.1}La_{0.45}Ca_{0.45}Fe_{11.7-x}Zn_xCo_{0.3}O_{19}$. The ratio of Fe and (CoZn) to (LaSrCa) was set at 10.6. And then, they were mixed together using wet ball milling in water for 6 h with a constant rotation velocity of 100 rpm and a ball to powder mass ratio of 12.5:1. The as-milled powders were dried and pre-calcined at 1250 °C for 2 h in air. As-calcined samples were pulverized again and then wet-milled with proper additives ($CaCO_3$, $SrCO_3$, SiO_2, and H_3BO_3) in water for 16 h to get powders with average particle size about 0.8 μm. The finely milled slurry was pressed into disk-shaped green pellets with Φ 35 × 15 mm under 200 MPa in the magnetic field of 1.2 T. Finally, the green compacts were sintered at 1190 °C for 1 h in air atmosphere.

The phase structures of the pre-calcined powders were detected by X-ray diffraction (DX-2700) with Cu K_α radiation ($\lambda=0.15418$ nm). The morphology of the sintered compacts were observed by field emission scanning electron microscopy (FEI Inspect F50). The Fe^{3+} sublattice occupation of the powders were investigated by ^{57}Fe Mössbauer spectroscopy (MS-500) at room temperature, using a ^{57}Co/Pd source. Magnetic properties of the sintered magnets were measured by a permanent magnetic measuring system (AMT-4).

3 Results and discussion

3.1 X-ray diffraction analysis

The X-ray diffraction patterns for the as-calcined magnetic powders with different Zn contents sintered at 1250 °C for 2 h in air are shown in Fig. 1. It was found from Fig. 1 that all the diffraction patterns were consistent with the standard pattern of $SrFe_{12}O_{19}$ (PDF: 80-1198), which suggested that all the magnetic powders possessed a single hexagonal ferrite phase with no observation of any impurity phases.

The lattice constants a and c are calculated from the values of d_{hkl} corresponding to (107) and (114) peaks according to the following formula [7]:

$$d_{hkl}=\left(\frac{4}{3}\cdot\frac{h^2+hk+k^2}{a^2}+\frac{l^2}{c^2}\right)^{-\frac{1}{2}} \quad (1)$$

where d_{hkl} is the interplanar crystal spacing, and h, k and l are the Miller indices.

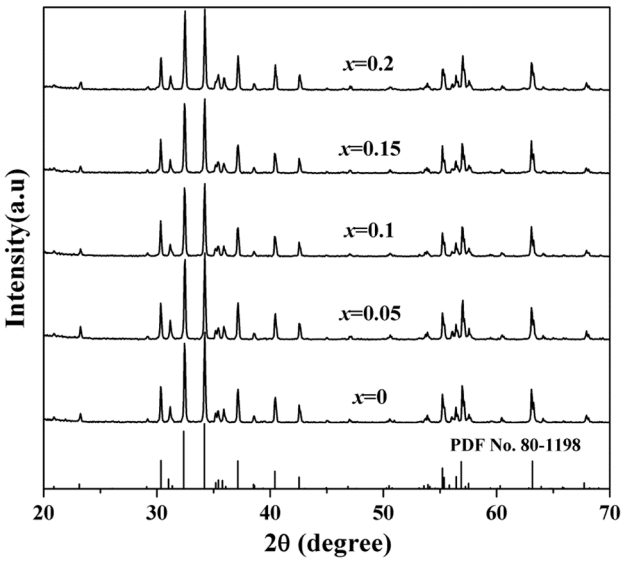

Fig. 1 X-ray diffraction patterns of Sr-hexaferrites ($x=0$, 0.05, 0.1, 0.15 and 0.2)

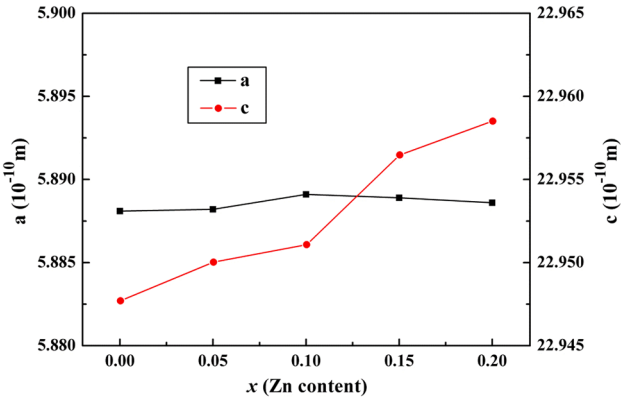

Fig. 2 Variation of lattice parameters as a function of Zn content in Sr-hexaferrites ($x=0$, 0.05, 0.1, 0.15 and 0.2)

Figure 2 shows the variations of the lattice constants a and c according to the doping content x. It can be seen that the lattice parameter c increased continuously with increase of x from 0 to 0.2, however, the values of lattice constant a had hardly changed compared with the lattice constant c. The variation in lattice parameter c could be explained on the basis of differences in ionic radii of Zn^{2+} (0.74 Å) and Fe^{3+} (0.645 Å). In addition, Zn^{2+} ions substitution led to the conversion of Fe^{3+} (0.645 Å) to Fe^{2+} (0.80 Å) to satisfy the total charge neutrality, which contributed to the lattice expansion [29].

3.2 Mössbauer spectroscopy

The sublattice occupation of Fe^{3+} ions can be determined from Mössbauer spectroscopy. 24 Fe^{3+} ions of the M-type hexagonal ferrites are distributed into five different sites: three octahedral sites (12*k*, 2*a* and $4f_2$), one tetrahedral site ($4f_1$) and one bipyramidal site (2*b*). Because of the coupling by super exchange interactions through the O^{2-} ions, 2*a*, 2*b* and 12*k* are arranged parallel to the *c*-axis, while $4f_1$ and $4f_2$ are antiparallel arrangement. The fitted room temperature ^{57}Fe Mössbauer spectra of $Sr_{0.1}La_{0.45}Ca_{0.45}Fe_{11.7-x}Zn_xCo_{0.3}O_{19}$ are shown in Fig. 3. And the hyperfine parameters are presented in Table 1. The spectra for all studied samples (Fig. 3) exhibited the splitting of the 12*k* component. A new component was developed, obtaining the hyperfine field values of about 400 kOe and isomer shift and quadrupole splitting less than that of 12*k* component (Table 1), which was assigned to 12*k* sites perturbed by the presence of other ions in neighboring sites, and named $12k_1$. Lee's study demonstrated that Zn^{2+} ions preferred to occupy $4f_1$ site [30]. However, as reported by Du, Zn^{2+} ions should occupy $4f_2$ site [31]. The areas of Mössbauer spectra sextets of Zn-doped Sr-hexaferrite series suggested that the site areas of both $4f_1$ and $4f_2$ decreased, compared with un-doped sample. These results indicated that Zn^{2+} ions occupied both $4f_1$ and $4f_2$ sites. However, the site area of $4f_1$ decreases lightly with increasing Zn content *x*, while $4f_2$ reduces monotonically as presented in Table 1, which showed that Zn^{2+} ions would preferentially occupy $4f_2$ site. This result might be explained that the $4f_2$ site is close to the La^{3+} ions, which is conducive to the reduction of electrostatic energy [31]. The splitting of the 12*k* component was induced by local cancellation of the $12k–4f_2$ super exchange interactions, which was due to substitution of non-magnetic ions or reduction of net magnetic moment [32, 33]. For $Sr_{0.1}La_{0.45}Ca_{0.45}Fe_{11.7-x}Zn_xCo_{0.3}O_{19}$ ($x=0$), as La^{3+} ions replaced Sr^{2+} ions, Fe^{3+} (5 μ_B) ions would be reduced to Fe^{2+} (4 μ_B) ions, to satisfy the total charge neutrality. Fe^{2+} ions was present in the close vicinity of the 12*k* site [5] and the La–Co cations preferred to occupy the $4f_2$, 12*k*, and 2*b* sites [12], which resulted in weakening of the $12k–4f_2$ super exchange interactions. On the other hand, Zn^{2+} (0 μ_B) ions preferentially occupied the $4f_2$ site, which led to further declining of the $12k–4f_2$ super exchange interactions, so that the splitting of the 12*k* component became more serious.

3.3 Electron microscopy

Figure 4 shows the FE-SEM micrographs of the $Sr_{0.1}La_{0.45}Ca_{0.45}Fe_{11.7-x}Zn_xCo_{0.3}O_{19}$ magnets with different Zn-substituted amount (*x*) at 1190 °C in air. It can be seen from the images that the sintered magnets have formed hexagonal or irregular structure and the particles were distributed relatively homogeneously. The mean particle sizes of the sintered magnets were not changed obviously with increase of Zn content. However, the radius–thickness ratio of the particle increased, compared with the magnet without Zn-doped.

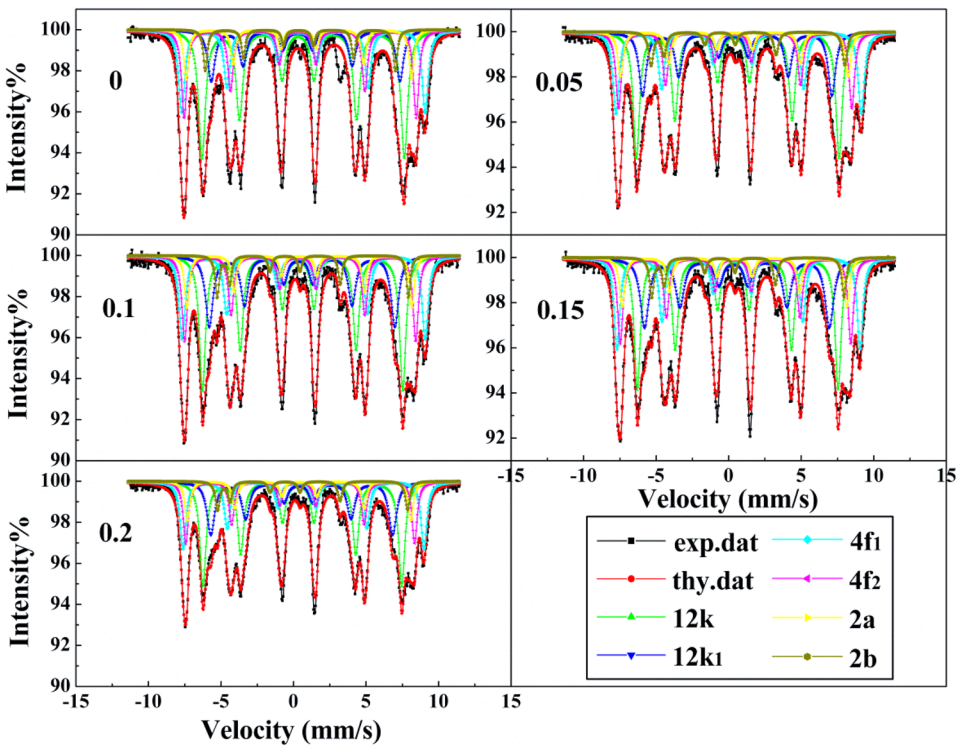

Fig. 3 Room temperature Mössbauer spectra of Sr-hexaferrites ($x=0$, 0.05, 0.1, 0.15 and 0.2)

Table 1 The isomer shift (δ), quadruple splitting (Q_S), hyperfine field values (H_{hf}), and percentage relative area (R_A), and sites of Fe^{3+} ions for $Sr_{0.1}La_{0.45}Ca_{0.45}Fe_{11.7-x}Zn_xCo_{0.3}O_{19}$ derived from Mössbauer spectra recorded at room temperature

Substitution (x)	Iron site	δ (mm/s)	Q_S (mm/s)	H_{hf} (kOe)	R_A (%)
0	12*k*	0.36 ± 0	0.31 ± 0.01	420.9 ± 0.6	34.0
	$12k_1$	0.35 ± 0.01	0.27 ± 0.03	401.9 ± 1	13.7
	$4f_1$	0.36 ± 0.01	0.42 ± 0.02	520.8 ± 1	19.4
	$4f_2$	0.27 ± 0.01	0.17 ± 0.02	495.4 ± 0.9	17.2
	2*a*	0.27 ± 0.02	0.04 ± 0.04	481.3 ± 1	10.0
	2*b*	0.24 ± 0.02	1.92 ± 0.05	409.9 ± 1	5.8
0.05	12*k*	0.37 ± 0	0.29 ± 0.01	433.1 ± 0.5	30.8
	$12k_1$	0.35 ± 0.01	0.26 ± 0.03	404.5 ± 1	17.8
	$4f_1$	0.37 ± 0.01	0.42 ± 0.02	524.2 ± 0.8	19.4
	$4f_2$	0.26 ± 0.01	0.15 ± 0.03	498.4 ± 0.8	16.2
	2*a*	0.29 ± 0.02	0.02 ± 0.04	486.3 ± 1	9.5
	2*b*	0.26 ± 0.02	1.92 ± 0.05	414.0 ± 1	6.2
0.1	12*k*	0.36 ± 0	0.30 ± 0.01	427.9 ± 0.6	30.4
	$12k_1$	0.35 ± 0.01	0.26 ± 0.03	395.4 ± 1	20.3
	$4f_1$	0.36 ± 0.01	0.46 ± 0.02	519.3 ± 1	18.4
	$4f_2$	0.26 ± 0.01	0.17 ± 0.02	494.3 ± 0.8	15.8
	2*a*	0.29 ± 0.01	0.02 ± 0.03	481.1 ± 1	9.2
	2*b*	0.27 ± 0.02	1.92 ± 0.04	408.3 ± 1	5.8
0.15	12*k*	0.36 ± 0	0.30 ± 0.01	429.1 ± 0.6	28.9
	$12k_1$	0.34 ± 0	0.24 ± 0.03	394.7 ± 1	20.7
	$4f_1$	0.35 ± 0	0.43 ± 0.02	519.2 ± 0.8	19.0
	$4f_2$	0.28 ± 0.01	0.17 ± 0.02	492.3 ± 1	15.5
	2*a*	0.30 ± 0.02	0.02 ± 0.04	480.0 ± 1	9.9
	2*b*	0.25 ± 0.02	1.94 ± 0.04	410.9 ± 1	6.1
0.2	12*k*	0.36 ± 0	0.29 ± 0.01	424.9 ± 0.6	30.8
	$12k_1$	0.34 ± 0.02	0.23 ± 0.03	388.7 ± 1	19.5
	$4f_1$	0.35 ± 0.01	0.45 ± 0.02	514.9 ± 0.9	18.9
	$4f_2$	0.26 ± 0.01	0.17 ± 0.02	488.9 ± 1	15.3
	2*a*	0.28 ± 0.02	0.02 ± 0.04	477.3 ± 1	9.5
	2*b*	0.26 ± 0.02	1.90 ± 0.05	405.9 ± 2	6.0

3.4 Magnetic properties

The room temperature hysteresis curves of Sr-hexaferrites doped with different amount of Zn content (x) are shown in Fig. 5. The remanence (B_r), magnetic induction coercivity (H_{cb}), intrinsic coercivity (H_{cj}) and maximum energy product [$(BH)_{max}$] of the magnets were determined from the obtained hysteresis curves. Then, the variations of B_r, H_c and $(BH)_{max}$ of the magnets would be analyzed in detail.

Figure 6 shows the effect of Zn content (x) on the remanence (B_r) of the hexaferrite $Sr_{0.1}La_{0.45}Ca_{0.45}Fe_{11.7-x}Zn_xCo_{0.3}O_{19}$ magnets. It can be seen that B_r of the sintered magnets increased from 434.9 mT (at $x=0$) to 440.6 mT (at $x=0.1$), then decreased with the Zn content (x) shifting from $x=0.1$ to $x=0.2$, and reached to 434.6 mT $(BH)_{max}$. The variation of B_r can be attributed to the substitution of Zn^{2+} ions into the down-spin sites of Fe^{3+} ions ($4f_1$ and $4f_2$), which has been determined according to the above Mössbauer analysis. As the substitution of Zn^{2+} ions for the Fe^{3+} ions at $4f_1$ and $4f_2$ sites, the net magnetic moment of the magnets at $x=0.05$ and 0.1 would increase, which led to increase in M_s due to the net magnetic moment being proportional to the magnetization, so B_r of the magnets increased. Furthermore, as shown in Fig. 6, the B_r decreased when x is above 0.1, which can be explained by the slight decrease of the net magnetic moment and the reduction of the Fe^{3+}–O–Fe^{3+} super exchange interaction due to the substitution of Zn^{2+} ions for Fe^{3+} ions [15]. These results indicated that the optimal amount of the Zn^{2+} addition could be beneficial to the improvement of the B_r, which is consistent with the previous reports [11, 14, 17].

Figure 7 depicts the change of the magnetic induction coercivity (H_{cb}) and intrinsic coercivity (H_{cj}) with Zn content (x) of $Sr_{0.1}La_{0.45}Ca_{0.45}Fe_{11.7-x}Zn_xCo_{0.3}O_{19}$ magnets. It can be seen clearly that H_{cb} and H_{cj} of the magnets continuously decreased with the increase of x from 0 to 0.2. The values of H_{cb} decreased from 326.2 kA/m (at $x=0$) to 178.6 kA/m (at $x=0.2$), and the values of H_{cj} dropped from 439.3 kA/m (at $x=0$) to 187.9 kA/m (at $x=0.2$), respectively. It is well known that the coercivity of the magnets depends on their magneto-crystalline anisotropy and microstructure. According to the literature [1], the coercivity could be expressed by the following equation:

$$Hc = \alpha Ha - \frac{N\left(B_r + J_s^0\right)}{\mu_0} \tag{2}$$

where α is the grain size factor, *H*a is the magneto-crystalline anisotropy field, *N* is the grain demagnetization factor, J_s^0 is the saturation of the magnet. The factor α increases with the decreasing grain size; the factor *N* increases when the grain shape becomes more platelet. As shown in Fig. 4, the FESEM micrographs exhibited that the particle size of the magnets did not change basically with increasing Zn contents, while the grain morphology became more platelet shaped, which demonstrated that the factor α remained constant and *N* increased. On the other hand, Mössbauer spectra indicated that Zn^{2+} ions occupied both $4f_1$ and $4f_2$ sites. The substitution of non-magnetic Zn^{2+} ions not only eliminates the contribution of magnetic Fe^{3+} ions to the magneto-crystalline anisotropy, but also weakens the super exchange interaction [27], which results in the reduction of the magneto-crystalline anisotropy. Therefore, the coercivity of the magnets monotonously decreased with the increase of Zn content (x).

The maximum energy product [$(BH)_{max}$] of the $Sr_{0.1}La_{0.45}Ca_{0.45}Fe_{11.7-x}Zn_xCo_{0.3}O_{19}$ magnets with different Zn content (x) are shown in Fig. 8. It can be seen

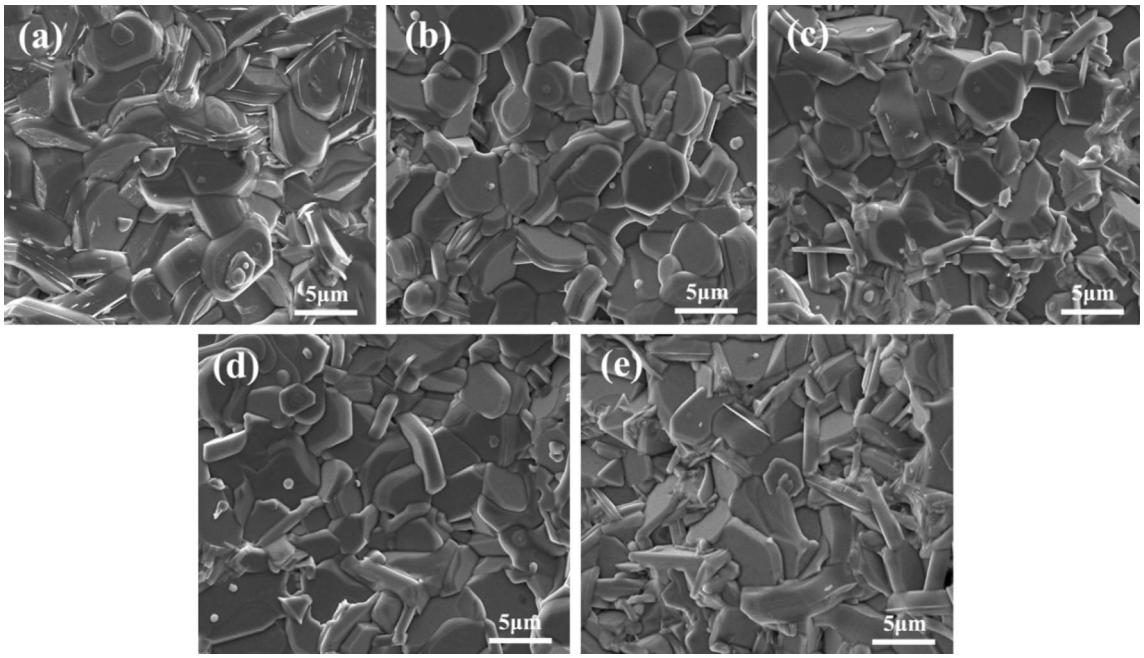

Fig. 4 FE-SEM micrographs of Sr-hexaferrites with **a** $x=0$, **b** $x=0.05$, **c** $x=0.1$, **d** $x=0.15$, **e** $x=0.2$

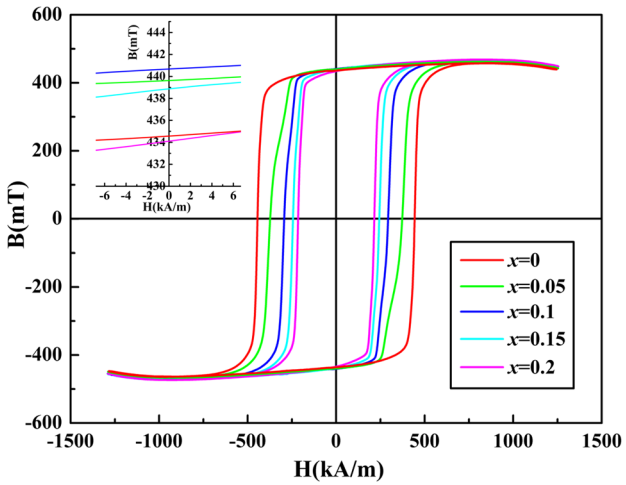

Fig. 5 Room temperature hysteresis curves of Sr-hexaferrites ($x=0$, 0.05, 0.1, 0.15 and 0.2)

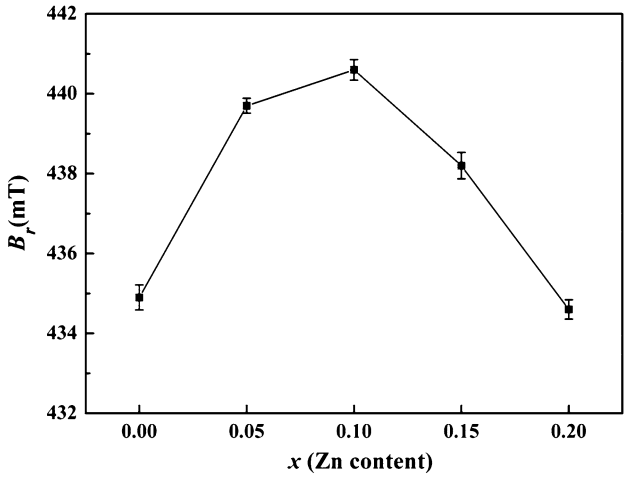

Fig. 6 The influence of the Zn content on B_r values of Sr-hexaferrites ($x=0$, 0.05, 0.1, 0.15 and 0.2)

that $(BH)_{max}$ had the similar feature as that of B_r, which increased firstly and then decreased, but it reached the maximum value of 36.88 kJ/m^3 at $x=0.05$ due to the inconsistency between the variation trends of the values of B_r and H_{cj}. Since $(BH)_{max}$ of the magnets was estimated by the product between the coercivity and remanent magnetization, and is considered as a comparative indication of the hysteresis area, the values of B_r and H_{cj} will have their influence on it.

4 Conclusions

$Sr_{0.1}La_{0.45}Ca_{0.45}Fe_{11.7-x}Zn_xCo_{0.3}O_{19}$ ($x=0$, 0.05, 0.1, 0.15 and 0.2) ferrite series were successfully prepared and systematically investigated in the present study. Ferrites with different Zn substitutions were all composed of single M-type phase, the lattice constant c increased and the particle shape became more platelet shaped with

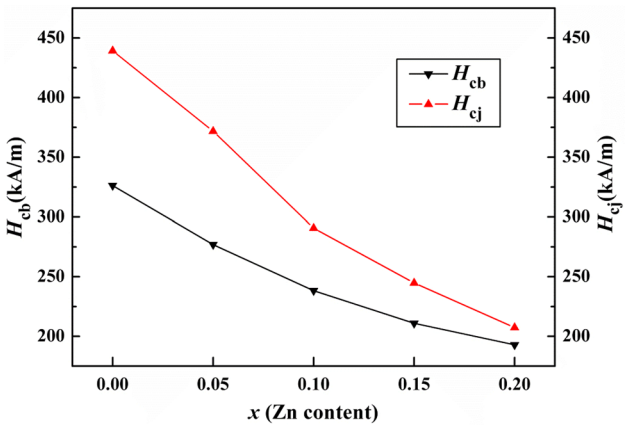

Fig. 7 The influence of the Zn content on H_{cb} and H_{cj} values of Sr-hexaferrites ($x=0$, 0.05, 0.1, 0.15 and 0.2)

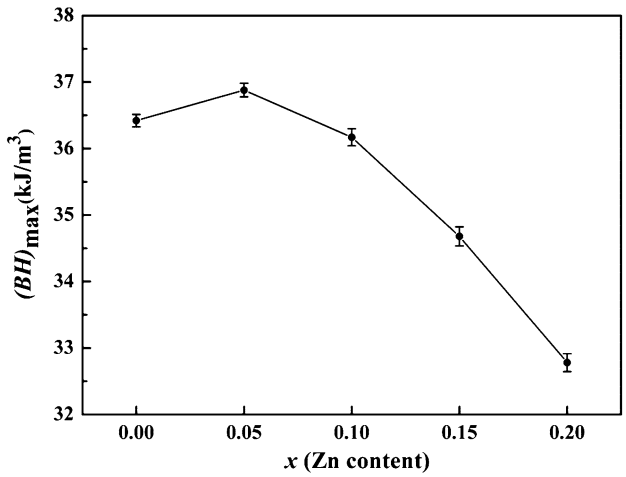

Fig. 8 The influence of the Zn content on $(BH)_{max}$ values of Sr-hexaferrites ($x=0$, 0.05, 0.1, 0.15 and 0.2)

increasing Zn substitution. The Mössbauer spectra for all samples demonstrated the splitting of the 12*k* component, and indicated that Zn^{2+} ions occupied both $4f_1$ and $4f_2$ sites, whereas Zn^{2+} ions would prefer to occupying $4f_2$ sites with increasing Zn substitution. Therefore, Zn substitution could slightly improve the remanence of the magnets at Zn content $x \leq 0.1$, while the intrinsic coercive force of the ferrites continuously decreased with Zn substitution. In addition, Zn substitution reduced the maximum energy product when Zn content x was larger than 0.05. Thus, it is recommended that the substitution amount of Zn is about 0.05.

Acknowledgements This work is supported by the Science and Technology Support Program of Sichuan Province (Grant No. CDWA2016ZC3-3).

References

1. F. Kools, A. Morel, R. Grössinger, J.M. Le Breton, P. Tenaud, LaCo-substituted ferrite magnets, a new class of high-grade ceramic magnets; intrinsic and microstructural aspects. J. Magn. Magn. Mater. **242–245**, 1270–1276 (2002)
2. M.M. Hessien, M.M. Rashad, M.S. Hassan, K. El-Barawy, Synthesis and magnetic properties of strontium hexaferrite from celestite ore. J. Alloy. Compd. **476**, 373–378 (2009)
3. T. Koutzarova, S. Kolev, C. Ghelev, I. Nedkov, B. Vertruen, R. Cloots, C. Henrist, A. Zaleski, Differences in the structural and magnetic properties of nanosized barium hexaferrite powders prepared by single and double microemulsion techniques. J. Alloy. Compd. **579**, 174–180 (2013)
4. X. Liu, W. Zhong, S. Yang, Z. Yu, B. Gu, Y. Du, Influences of La^{3+} substitution on the structure and magnetic properties of M-type strontium ferrites. J. Magn. Magn. Mater. **238**, 207–214 (2002)
5. J.M. Le Breton, D. Seifert, J. Töpfer, L. Lechevallier, A Mössbauer investigation of $Sr_{1-x}La_xFe_{12}O_{19}$ ($0 \leq x \leq 1$) M-type hexaferrites. Phys. B **470–471**, 33–38 (2015)
6. C. Lei, S. Tang, Y. Du, Synthesis of aligned La^{3+}-substituted Sr-ferrites via molten salt assisted sintering and their magnetic properties. Ceram. Int. **42**(14), 15511–15516 (2016)
7. P. Sharma, A. Verma, R.K. Sidhu, O.P. Pandey, Influence of Nd^{3+} and Sm^{3+} substitution on the magnetic properties of strontium ferrite sintered magnets. J. Alloy. Compd. **361**, 257–264 (2003)
8. Z. Wang, Z. Zhou, W. Zhang, H. Qian, M. Jin, Preparation and Magnetic Properties of Nd^{3+}, Al^{3+}, Ca^{2+} Substituted M-Type Strontium Hexaferrites. J. Supercond. Nov. Magn. **26**, 3501–3506 (2013)
9. S. Katlakunta, S.S. Meena, S. Srinath, M. Bououdina, R. Sandhya, K. Praveena, Improved magnetic properties of Cr^{3+} doped $SrFe_{12}O_{19}$ synthesized via microwave hydrothermal route. Mater. Res. Bull. **63**, 58–66 (2015)
10. Y. Yang, F. Wang, X. Liu, J. Shao, S. Feng, D. Huang, M. Li, The effect of Bi substitution on the microstructure and magnetic properties of the $Sr_{0.4}Ba_{0.3}La_{0.3}Fe_{12-x}Bi_xO_{19}$ hexagonal ferrites. J. Magn. Magn. Mater. **422**, 209–215 (2017)
11. A. Baykal, I.A. Auwal, S. Güner, H. Sözeri, Magnetic and optical properties of Zn^{2+} ion substituted barium hexaferrites. J. Magn. Magn. Mater. **430**, 29–35 (2017)
12. D.H. Choi, S.W. Lee, I.-B. Shim, C.S. Kim, Mössbauer studies for La–Co substituted strontium ferrite. J. Magn. Magn. Mater. **304**, e243–e245 (2006)
13. L. Peng, L. Li, R. Wang, Y. Hu, X. Tu, Effect of La–Co substitution on the crystal structure and magneticproperties of hot press sintered $Sr_{1-x}La_xFe_{12-x}Co_xO_{19}$ ($x=0$–0.5) ferrites for use in LTCC technology. J. Magn. Magn. Mater. **391**, 136–139 (2015)
14. Z.H. Hua, S.Z. Li, Z.D. Han, D.H. Wang, M. Lu, W. Zhong, B.X. Gu, Y.W. Du, The effect of La–Zn substitution on the microstructure and magnetic properties of barium ferrites. Mater. Sci. Eng. A **448**, 326–329 (2007)
15. P. Kumar, A. Gaur, Room temperature magneto-electric coupling in La–Zn doped $Ba_{1-x}La_xFe_{12-x}Zn_xO_{19}$ ($x = 0.0$–0.4) hexaferrite. Appl. Phys. A **123**, 732 (2017)
16. L. Qiao, L. You, J. Zheng, L. Jiang, J. Sheng, The magnetic properties of strontium hexaferrites with La–Cu substitution prepared by SHS method. J. Magn. Magn. Mater. **318**, 74–78 (2007)
17. Y.-M. Kang, Y.-H. Kwon, M.-H. Kim, D.-Y. Lee, Enhancement of magnetic properties in Mn–Zn substituted M-type Sr-hexaferrites. J. Magn. Magn. Mater. **382**, 10–14 (2015)
18. Y. Yang, J. Shao, F. Wang, X. Liu, D. Huang, Impacts of MnZn doping on the structural and magnetic properties of M-type SrCaLa hexaferrites. Appl. Phys. A **123**(5), 310 (2017)

19. C. Singh, S.B. Narang, I.S. Hudiara, Y. Bai, K. Marina, Hysteresis analysis of Co–Ti substituted M-type Ba–Sr hexagonal ferrite. Mater. Lett. **63**, 1921–1924 (2009)
20. Z. Zhang, X. Liu, X. Wang, Y. Wu, R. Li, Effect of Nd–Co substitution on magnetic and microwave absorption properties of $SrFe_{12}O_{19}$ hexaferrites. J. Alloy. Compd. **525**, 114–119 (2012)
21. J.M. Le Breton, J. Teillet, G. Wiesinger, A. Morel, F. Kools, P. Tenaud, Mössbauer Investigation of Sr–Fe–O Hexaferrites With La–Co Addition. IEEE Trans. Magn. **38**, 2952–2954 (2002)
22. A. Morel, J.M. Le Breton, J. Kreisel, G. Wiesinger, F. Kools, P. Tenaud, Sublattice occupation in $Sr_{1-x}La_xFe_{12-x}Co_xO_{19}$ hexagonal ferrite analyzed by Mössbauer spectrometry and Raman spectroscopy. J. Magn. Magn. Mater. **242–245**, 1405–1407 (2002)
23. G. Wiesinger, M. Müller, R. Grössinger, M. Pieper, A. Morel, F. Kools, P. Tenaud, J.M. Le Breton, J. Kreisel, Substituted ferrites studied by nuclear methods. Phys. Stat. Sol. (a) **189**, 499–508 (2002)
24. L. Lechevallier, J.M. Le Breton, J. Teillet, A. Morel, F. Kools, P. Tenaud, Mössbauer investigation of $Sr_{1-x}La_xFe_{12-y}Co_yO_{19}$ ferrites. Phys. B **327**, 135–139 (2003)
25. X. Li, W. Yang, D. Bao, X. Meng, B. Lou, Influence of Ca substitution on the microstructure and magnetic properties of SrLaCo ferrite. J. Magn. Magn. Mater. **329**, 1–5 (2013)
26. Y. Yang, X. Liu, D. Jin, Y. Ma, Structural and magnetic properties of La–Co substituted Sr–Ca hexaferrites synthesized by the solid state reaction method. Mater. Res. Bull. **59**, 37–41 (2014)
27. X. Huang, X. Liu, Y. Yang, K. Huang, X. Niu, D. Jin, S. Gao, Y. Ma, F. Huang, F. Lv, S. Feng, Microstructure and magnetic properties of Ca-substituted M-type SrLaCo hexagonal ferrites. J. Magn. Magn. Mater. **378**, 424–428 (2015)
28. Z. Chen, F. Wang, S. Yan, Z. Feng, Microstructure and magnetic properties of M-type $Sr_{0.61-x}La_{0.39}CaxFe_{11.7}Co_{0.3}O_{19}$ hexaferrite prepared by microwave calcination. Mater. Sci. Eng. B **182**, 69–73 (2014)
29. B.K. Rai, S.R. Mishra, V.V. Nguyen, J.P. Liu, Synthesis and characterization of high coercivity rare-earth ion doped $Sr_{0.9}RE_{0.1}Fe_{10}Al_2O_{19}$ (RE: Y, La, Ce, Pr, Nd, Sm, and Gd). J. Alloy. Compd. **550**, 198–203 (2013)
30. S.W. Lee, S.Y. An, I.-B. Shim, C.S. Kim, Mössbauer studies of La–Zn substitution effect in strontium ferrite nanoparticles. J. Magn. Magn. Mater. **290–291**, 231–233 (2005)
31. Y. Du, H. Lu, Y. Zhang, L. Hui, T. Wang, Investigation of magnetic properties and Mössbauer spectra of $La_xBa_{1-x}Fe_{12-x}Zn_xO_{19}$ ferrites. Acta. Phys. Sin. **32**, 168–175 (1983). **(In Chinese)**
32. M. Awawdeh, I. Bsoul, S.H. Mahmood, Magnetic properties and Mössbauer spectroscopy on Ga, Al, and Cr substituted hexaferrites. J. Alloy. Compd. **585**, 465–473 (2014)
33. I. Bsoul, S.H. Mahmood, A.-F. Lehlooh, A. Al-Jamel, Structural and magnetic properties of $SrFe_{12-2x}Ti_xRu_xO_{19}$. J. Alloy. Compd. **551**, 490–495 (2013)